ADVANCED FUNCTIONAL MATERIALS
www.afm-journal.de

Inducing Endoplasmic Reticulum Stress to Expose Immunogens: A DNA Tetrahedron Nanoregulator for Enhanced Immunotherapy

Yanhua Li, Xia Zhang, Xiuyan Wan, Xiaohan Liu, Wei Pan, Na Li, and Bo Tang**

Immunogenic cell death (ICD) is an important modulation type for stimulating anticancer immune responses and amplifying immunotherapy efficacy. When ICD occurs, endoplasmic reticulum (ER) stress plays a vital role for exposing immunogens. Herein, a functionalized DNA tetrahedron nanoregulator to specifically trigger ER stress for enhancing cancer immunotherapy is designed. The nanoregulator can target ER organelles by binding to the sulfonamide receptor of cancer cells. Then glucose depletion and reactive oxygen species generation cause a strong ER stress response to induce ICD to expose tumor immunogens. Thereafter, the dendritic cell (DC) maturation is promoted, and T cell proliferation and infiltration are stimulated to advance cancer immunotherapy. Combined with immune checkpoint inhibitor (α-PD-1), the ER stress triggered nanoregulator exhibits significant suppression for breast cancer and melanoma.

1. Introduction

Cancer immunotherapy, which harnesses the host's own immune systems to fight cancer, has emerged as the most potential cancer therapeutic strategy.[1] Nevertheless, this treatment always suffers from a low response rate mainly due to the poor tumor immunogenicity and immunosuppressive microenvironment.[2] Recently, extensive efforts have been devoted for improving the immunogenicity of cancer cells to stimulate the anticancer immune response and enhance the therapeutic efficacy of immunotherapy.[3] Immunogenic cell death (ICD) is a new cell death pattern with the characteristic that the dying cancer cells can express or release death association molecular patterns (DAMPs) to induce anti-tumor immune effect. When ICD occurs, the early cell surface exposure of calreticulin (CRT) proteins will appear as the "eat me" signals to promote the dendritic cell (DC) maturation. Then the later release of high mobility group box 1 (HMGB1) will bind specifically to Toll-like receptor 4 on the surface of DC to optimally present antigens from dying tumor cells.[4] The increased antigens by ICD are the own signals of dying cells, which is beneficial for treating the extremely diverse and heterogeneous cancers.[5] Many ICD inducers: endoplasmic reticulum (ER) stress-independent or ER stress-dependent have been studied for anticancer therapy.[6] Among them, ER stress-dependent ICD inducers (e.g., anthracyclines, oxaliplatin, irradiation) are widely applied due to the high ICD-induction efficiency.[7] Significantly, it has been reported that the oxidative stress in organelles can induce enhanced ICD and increase more immunogen exposure.[8] Furthermore, the increased immunogens caused by ICD are mainly due to exposing CRT proteins of ER to the cell surface, which are directly resulted from ER stress. Overall, developing a strategy that directly stimulates ER stress in ER for upregulating CRT proteins on the cell surface is more effective for enhancing cancer immunotherapy.

Many disturbances, including cellular redox regulation, glucose deprivation, aberrant Ca^{2+} regulation, and viral infection, can directly lead to ER stress of cells.[9] Glucose oxidase (Gox),[10] a typical endogenous redox enzyme with inherent biocompatibility, can efficiently catalyze the conversion of glucose into gluconic acid and hydrogen peroxide (H_2O_2). The glucose depletion and reactive oxygen species (ROS) generation in ER can stimulate intense ER stress. To introduce Gox into the ER organelles of cancer cells, rational drug delivery systems (DDSs)[11] should be designed. DNA nanocarriers have been widely applied in DDSs due to their biocompatibility, programmability, well-defined structures, and precise-modified sites. Among these, the DNA tetrahedron with simple synthesis procedure and high yield, has captured great attentions for transporting functional drugs and proteins.[12] Such DNA tetrahedron with appropriate size provides good access to accumulate in ER with assistance of targeting groups.

Herein, we present a functionalized DNA tetrahedron nanoregulator that can specifically induce ER stress for tumor immunogen exposure and enhanced immunotherapy. As schematically illustrated in **Scheme 1**, TsG is modified to Gox as the ER-targeted ligand for anchoring to the ER organelles by binding to the sulfonamide receptor of cells. Thereafter, the functional Gox is conjugated with DNA tetrahedron and further camouflaged by cancer cell membrane to form the nanoregulator. When the nanoregulator accumulates in ER organelles, the catalytic reaction initiated by Gox consumes glucose and

Y. Li, X. Zhang, X. Wan, X. Liu, Dr. W. Pan, Prof. N. Li, Prof. B. Tang
College of Chemistry
Chemical Engineering and Materials Science Key Laboratory of Molecular and Nano Probes
Ministry of Education Collaborative Innovation Center of Functionalized Probes for Chemical Imaging in Universities of Shandong
Institute of Molecular and Nano Science
Shandong Normal University
Jinan 250014, P. R. China
E-mail: lina@sdnu.edu.cn; tangb@sdnu.edu.cn

The ORCID identification number(s) for the author(s) of this article can be found under https://doi.org/10.1002/adfm.202000532.

DOI: 10.1002/adfm.202000532

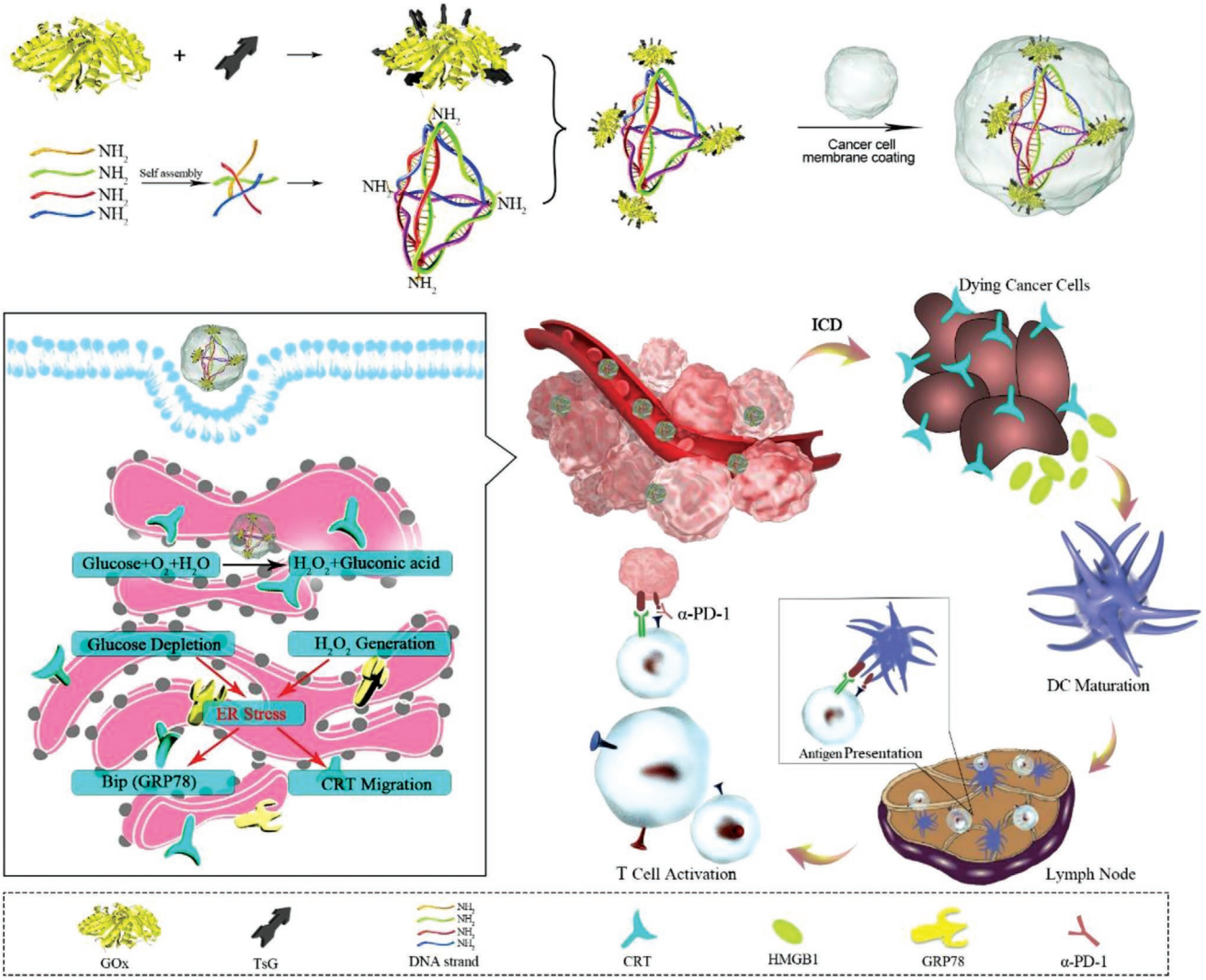

Scheme 1. Schematic illustration of preparation and application of DNA tetrahedron nanoregulator for enhanced cancer immunotherapy.

produces H_2O_2: glucose + O_2 → gluconic acid + H_2O_2. Notably, the upregulated glucose regulated protein 78 kD (GRP78) indicates that both glucose depletion and ROS generation in ER cause a strong ER stress response, which further induces the ICD of cancer cells to expose DAMPs. The exposed CRT proteins and HMGB1 promote the maturation of DCs by high expression of CD80 and CD86. Then DCs present antigens to stimulate T cell proliferation and infiltration to attack cancer cells. Combined with immune checkpoint inhibitor (α-PD-1), our nanoregulator significantly suppresses the growth of breast cancer and melanoma in tumor-bearing mice models.

2. Results and Discussion

2.1. Synthesis and Characterization of Nanoregulator (Td@Gox-TsG@C)

The nanoregulator that induces ER stress (Td@Gox-TsG@C) is constructed via three steps: 1) TsG, a relatively small ER target group, is modified with the Gox to form Gox-TsG; 2) Gox-TsG is linked to the aminated DNA tetrahedron to obtain Td@Gox-TsG; and 3) Td@Gox-TsG was coated with homologous cancer cell membrane to form Td@Gox-TsG@C.

In detail, methyl sulfonamide groups possess the ability to target to the ER.[13] And the methyl sulfonamide group and carboxyl group were linked together to construct an ER-targeted functional compound (TsG) (**Figure 1**A). The structure of TsG were characterized by ^{13}C-NMR, ^{1}H NMR, and mass spectrum (MS) (Figure S1, Supporting Information). Then the Gox is modified with TsG by the reaction between amino groups (of Gox) and carboxyl group (of TsG) to obtain Gox-TsG.

DNA nanostructures have been considered as excellent nanocarriers due to their benign biocompatibility and easy modification. To better locate in the organelle, we chose small-sized DNA tetrahedron as the nanocarrier. The aminated DNA tetrahedron was prepared by the reported method.[14] The obtained tetrahedron showed a sharp band on 4% PAGE gel (Figure 1B). The gel electrophoresis results revealed that the bands of S4, S4+S3, S4+S3+S2, and DNA tetrahedron appeared from bottom

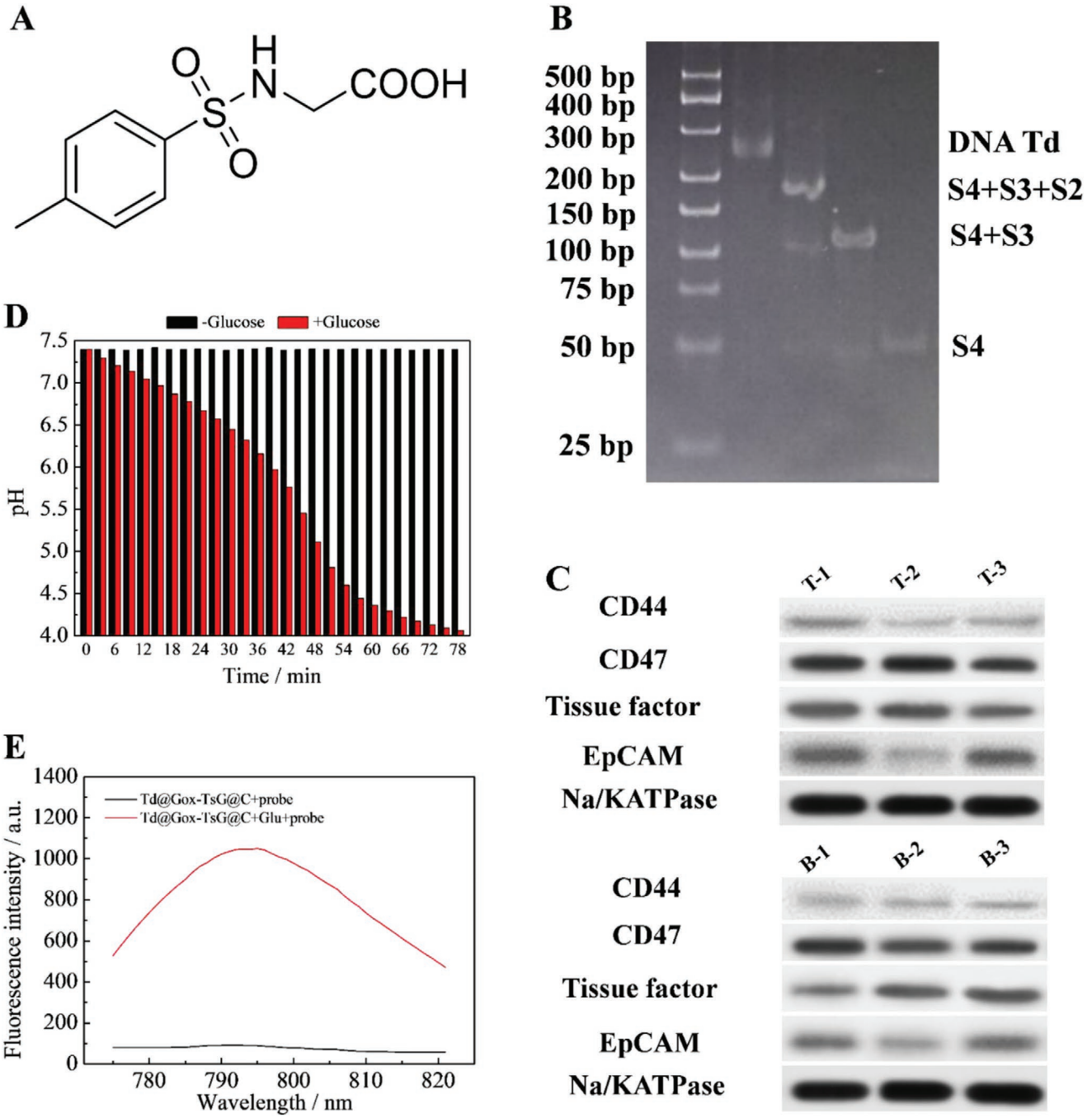

Figure 1. Characterization of materials. A) Structural formula of TsG. B) Gel electrophoresis imaging of DNA Td, S4+S3+S2, S4+S3, and S4; C) Western blotting assays of 4T1 cells (T-1), 4T1 cell membrane (T-2), Td@Gox-TsG@C (T-3), BF cells (B-1), BF cell membrane (B-2), Td@Gox-TsG@C (B-3), Na/KATPase as the internal reference; D) The pH values of Td@Gox-TsG@C solution in the presence or absence of glucose. E) Fluorescence spectra of Cy-O-Eb probe incubated with Td@Gox-TsG@C in the presence or absence of glucose.

to top in sequence (Figure 1B). Transmission electron microscopy (TEM) image showed that the DNA tetrahedron had homogeneous morphology with an average diameter at ≈7 nm (Figure S2, Supporting Information).

We subsequently loaded Gox-TsG onto the DNA tetrahedron to obtain Td@Gox-TsG (details of the synthesis are shown in the Experimental Section). Then the atomic force microscopy (AFM) images revealed that the size of the obtained Td@Gox-TsG was much larger than that of monodisperse DNA nanostructures (tetrahedron), which indicated the successful modification of Gox on tetrahedron (Figure S3A,B, Supporting Information). The materials without Gox or TsG were prepared as the control groups (named as Td@TsG or Td@Gox, respectively). Then Td@Gox-TsG@C were prepared by fusing cancer cell membrane with Td@Gox-TsG. Translocation of cancer cell membrane protein content, including CD44, CD47, tissue

factor, and EpCAM (major proteins associated with cancer cell invasion and metastasis), onto Td@Gox-TsG was examined by western blotting. Cancer cells and corresponding membrane were provided in parallel for comparison, and the bands of proteins in Figure 1C showed that the preparation of Td@Gox-TsG@C resulted in the retention of membrane proteins. Furthermore, a protein bicinchoninic acid (BCA) assay was employed to verify the cell membrane coating. Compared with DNA tetrahedrons (Td), Gox and cell membrane showed the obvious absorption peaks at 562 nm (Figure S4A,B, Supporting Information), indicating that the proteins existed in the samples. The stronger absorption of Td@Gox-TsG@C than Gox or cell membrane at 562 nm showed that more proteins existed in Td@Gox-TsG@C due to the Gox and membrane-bonded protein (Figure S4A,B, Supporting Information), indicating the successful coating of cell membrane.

2.2. Study on the Catalytic Property of Td@Gox-TsG@C

Gox, an efficient enzyme, can specifically catalyze the conversion of glucose into gluconic acid and H_2O_2: glucose + O_2 → gluconic acid + H_2O_2.[15] So we studied the catalytic activity of Td@Gox-TsG@C in presence of glucose by detecting pH value and H_2O_2. The pH value continually decreased from 7.40 to 4.06 during the process, which verified the generation of gluconic acid (Figure 1D). Cy-O-Eb,[16] a specific probe that fluoresced after reacting with H_2O_2, was employed in fluorescence analysis to verify the H_2O_2 produced during the catalytic process (Figure 1E). The above results indicated that the modified Gox in Td@Gox-TsG@C maintained high catalytic capacity.

2.3. ER Co-Localization

Confocal laser scanning microscopy (CLSM) assays were carried out to assess the ER targeting capability of the prepared materials. A commercial ER-targeted dye, ER-Tracker Red, was employed to locate the ER (red signal). The DNA tetrahedron used here was modified with FAM (green signal) to label our materials. When materials with TsG were added to cells, the red fluorescence and green fluorescence overlaps more than that without TsG. The corresponding pearson correlation coefficient (p value) were 0.512 for materials without TsG in 4T1 cells; 0.815 for materials with TsG in 4T1 cells; 0.391 for materials without TsG in BF cells; 0.812 for materials with TsG in BF cells, which suggested that the TsG played the crucial role in the ER targeting of the materials (**Figure 2**A,B). Flow cytometry assays also indicated that the fluorescence of ER-Tracker Red and FAM overlapped well and an obvious yellow signal was presented in the merged channel (Figure 2C,D).

2.4. Visualization of Intracellular H_2O_2 Accumulation

To verify the catalytic performance of Td@Gox-TsG, intracellular H_2O_2 accumulation was observed using DCFH-DA

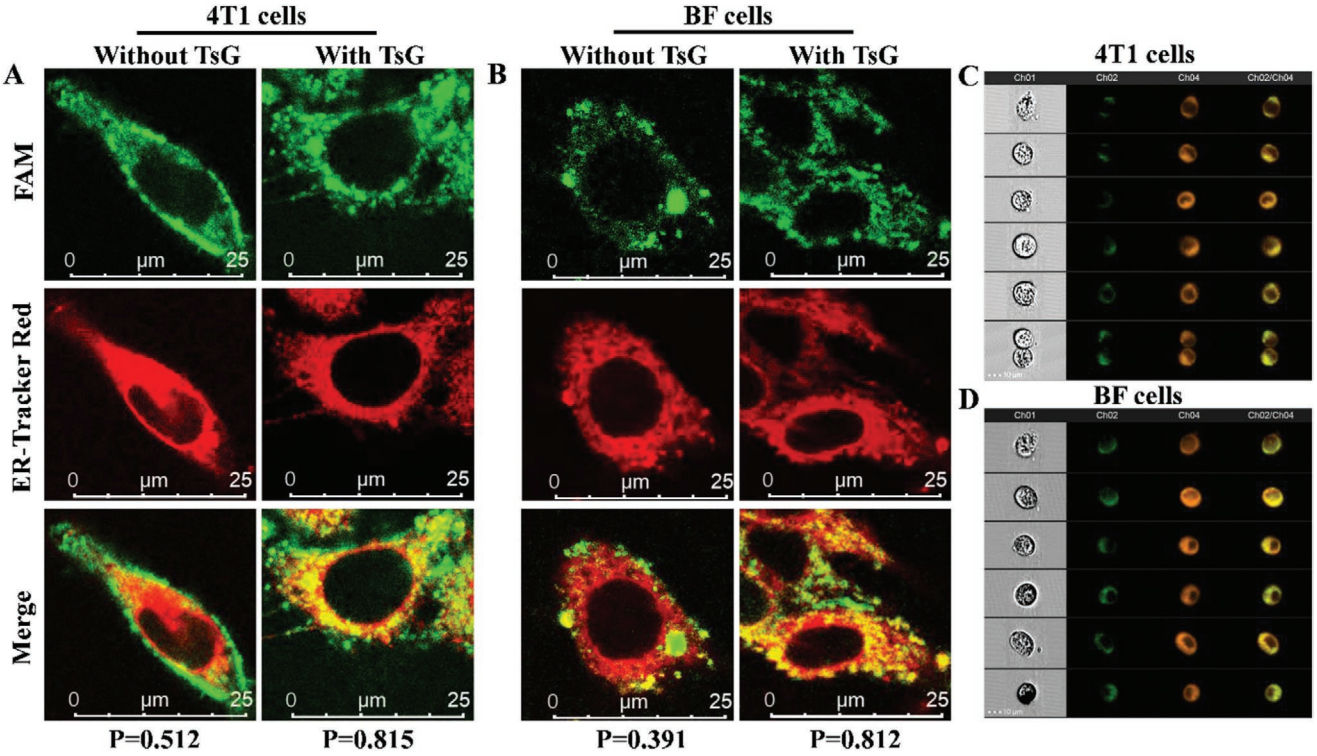

Figure 2. Endoplasmic reticulum (ER) co-localization. A) Confocal laser scanning microscopy (CLSM) images of 4T1 cells: left (without TsG); right (with TsG); B) CLSM images of BF cells: left (without TsG); right (with TsG); C) Flow cytometry of 4T1 cells (with TsG); D) Flow cytometry of BF cells (with TsG).

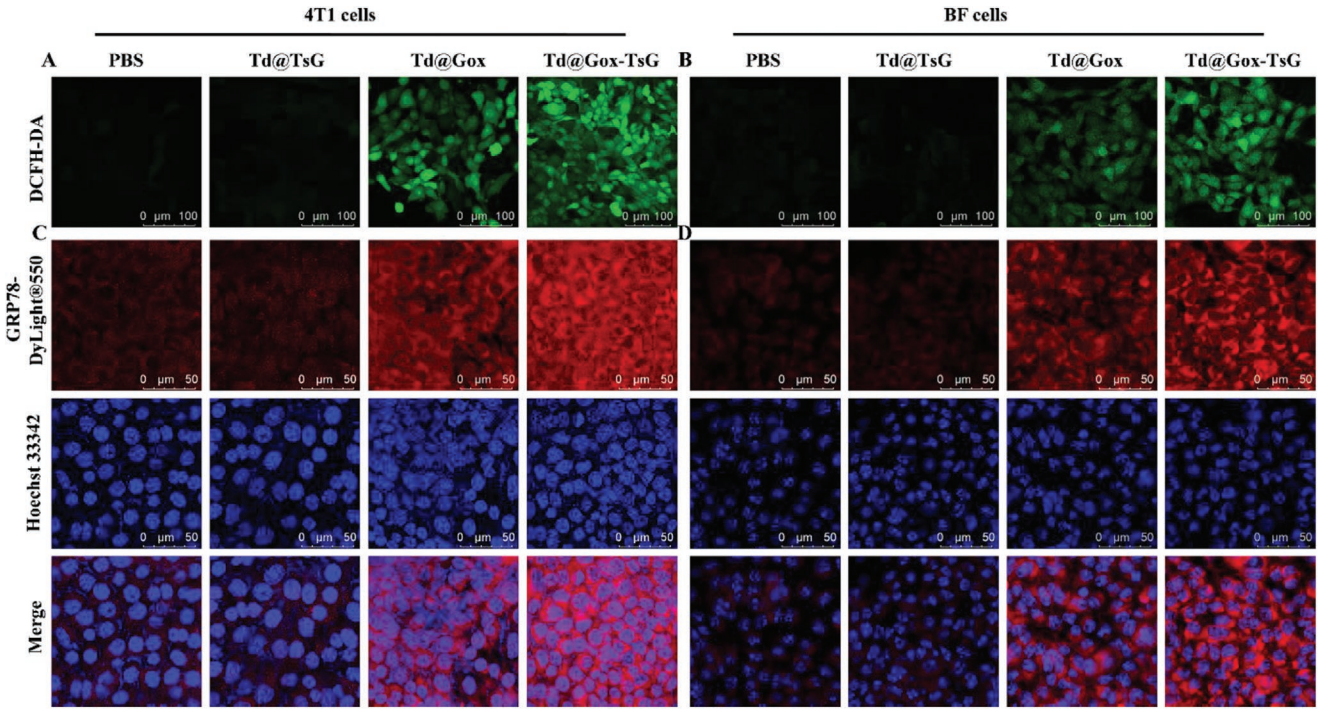

Figure 3. Verification of endoplasmic reticulum stress (ER stress). Detection of intracellular H_2O_2 after different treatments: A) 4T1 cells; B) BF cells. The immunofluorescence staining images of GRP78 after different treatments: C) 4T1 cells; D) BF cells.

probe after treated with PBS, Td@TsG, Td@Gox, and Td@Gox-TsG, respectively (**Figure 3**A,B). PBS and Td@TsG groups showed weak fluorescence signals in 4T1 or BF cells, indicating the little H_2O_2 accumulation. Td@Gox group showed stronger fluorescence intensity, due to that intracellular glucose was catalyzed by Gox to generate H_2O_2. Significantly, the highest fluorescence signals in Td@Gox-TsG group exhibited the most pronounced oxidative stress, mainly owing to the strong ER stress by Gox located in ER. The corresponding fluorescence intensities were shown in Figure S5, Supporting Information.

2.5. Verification of ER Stress

Glucose regulated protein 78 kD (GRP78), also called immunoglobulin heavy chain binding protein (Bip), is the main ER molecular chaperone.[17] The up-regulation of GRP78 is the specific marker of ER stress response. Therefore, GRP78 of 4T1 and BF cells was monitored by the immunofluorescence staining after treated with PBS, Td@TsG, Td@Gox, or Td@Gox-TsG to verify the emergence of ER stress. PBS and Td@TsG groups exhibited low fluorescence signal (Figure 3C,D), indicating that no ER stress occurred. The stronger fluorescence intensity of Td@Gox groups demonstrated that conspicuous ER stresses appeared due to the glucose consumption and ROS production by Gox (Figure 3C,D). Significantly, the strongest fluorescence signals of Td@Gox-TsG groups demonstrated that the ER stresses were more powerful on account of the catalytic reaction in ER (Figure 3C,D). The expression levels of GRP78 have been tested further by RT-PCR and western blotting. RT-PCR data in Figure S6A,B, Supporting Information, showed that Td@Gox can increase the expression of GRP78 due to the induced ER stress. Furthermore, the cells treated with Td@Gox-TsG expressed higher levels of GRP78 than that with Td@Gox, which indicated that ER stresses were more powerful (Figure S6A,B, Supporting Information). Data from western blotting assays also showed that the cells treated with Td@Gox-TsG expressed higher levels of GRP78 than that with Td@Gox, indicating that the stimulation in ER can cause the more intense ER stress (Figure S6E,F, Supporting Information). Above experimental results indicated that the stimulation triggered by Td@Gox-TsG in ER can successfully induce the enhanced ER stress in cells.

2.6. Determination of CRT Proteins

The induction of ICD depends on the exposure of CRT proteins.[4] During the process of ER stress, CRT proteins will migrate from ER lumen to the cell membrane as "eat-me" signals. As can be seen from **Figure 4**A,B, the red fluorescence signals of cells treated with Td@Gox were much stronger than that with PBS or Td@TsG, which resulted from the induced ER stress. Of note, the highest red signals of Td@Gox-TsG among the four groups showed the most CRT proteins owing to the strongest ER stress (Figure 4A,B). Flow cytometry analysis of CRT proteins also demonstrated the same experimental trend as above (Figure 4C–F). The expression level of CRT proteins were also tested by RT-PCR and western blotting. RT-PCR data in Figure S6C,D, Supporting Information, showed that Td@Gox can increase the expression of CRT due to the induced

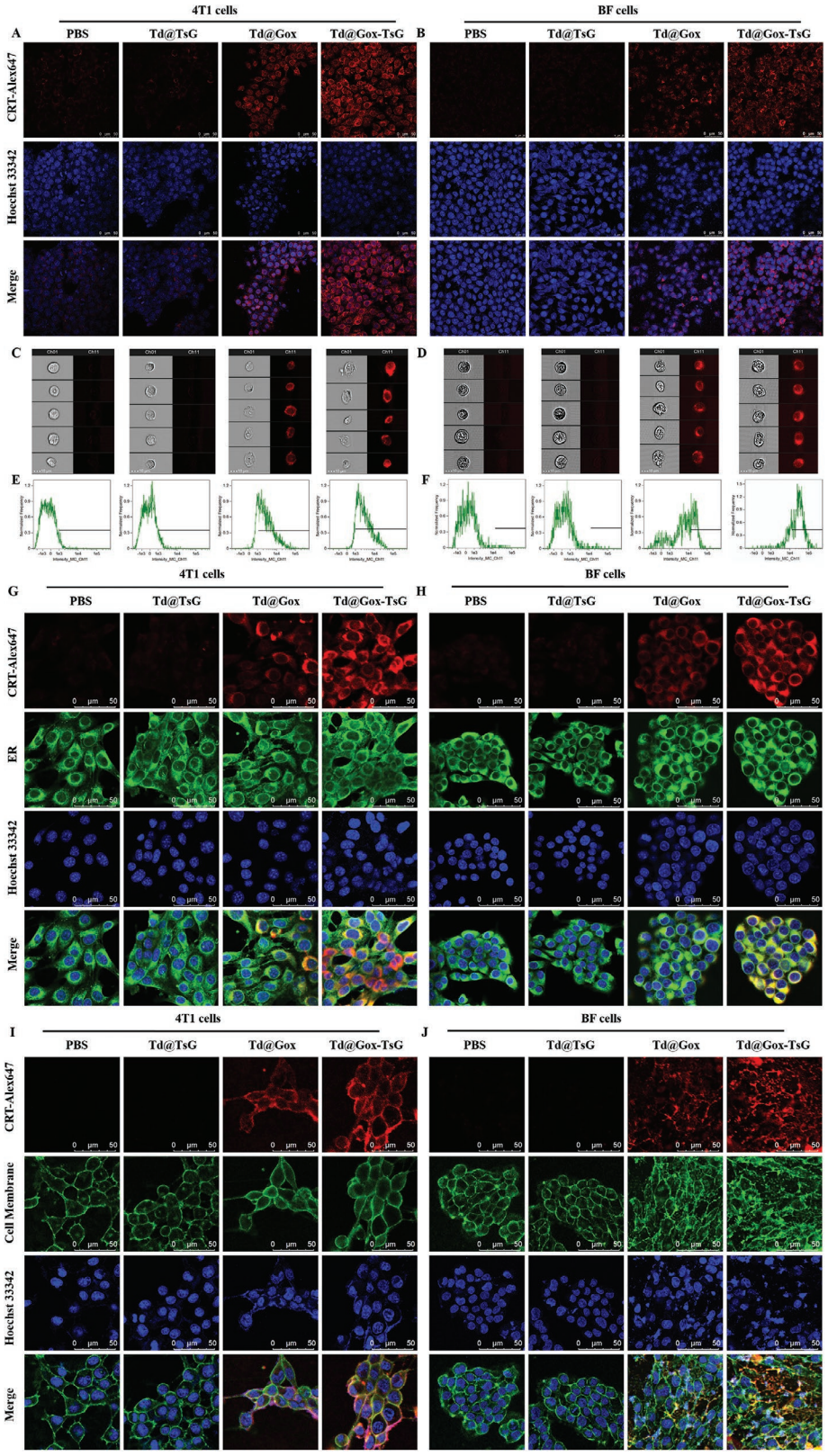

Figure 4. Determination of CRT proteins. Immunofluorescence staining images of CRT proteins after different treatments: A) 4T1 cells; B) BF cells; Flow cytometry images of CRT proteins: C) 4T1 cells; D) BF cells; Corresponding quantifications of fluorescence intensity: E) 4T1 cells; F) BF cells; G,H) The cells were permeated to study the co-location of CRT proteins with ER; I,J) And the cells were not permeated to study the co-location of CRT proteins with cell membrane.

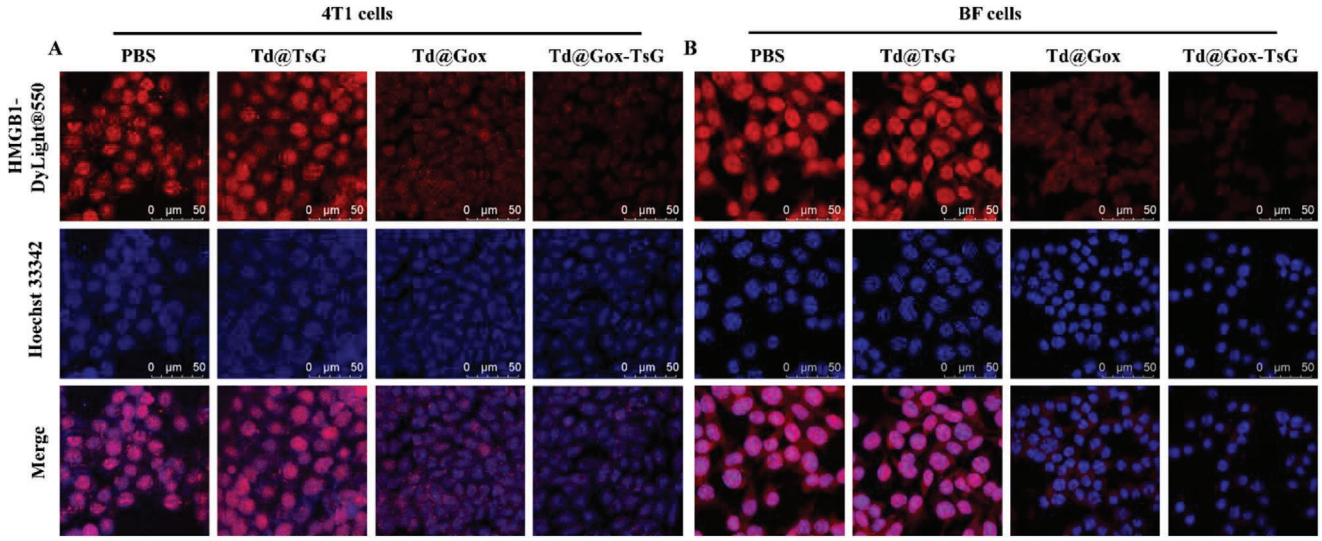

Figure 5. Examination of HMGB1. HMGB1-positive nuclear staining images after different treatments: A) 4T1 cells; B) BF cells.

ER stress. And the cells treated with Td@Gox-TsG expressed higher levels of CRT than that with Td@Gox, which indicated that ER stresses were more intense by directly stimulating the ER (Figure S6C,D, Supporting Information). Data from western blotting assays also showed that the cells treated with Td@Gox-TsG expressed higher levels of CRT than that with Td@Gox, indicating that the stimulation in ER can cause the more intense ER stress and ICD of cancer cells (Figure S6E,F, Supporting Information).

To test the exposure of CRT proteins from the ER to the cell membrane after various treatment, the co-location of CRT proteins with ER and cell membrane have been studied by CLSM. The co-location of CRT proteins and ER was first studied. Cells were fixed and permeated before treated with blocking reagent, and following by incubation with anti-CRT-Alex 647, ER tracker, and Hoechst 33 342, successively. The results (Figure 4G,H) showed that the CRT (red) and the ER (green) have good co-localization effect, indicating that the CRT proteins express mainly in the ER after treated with Td@Gox and Td@Gox-TsG. And the stronger fluorescence signals of cells treated with Td@Gox-TsG than with Td@Gox indicated that Td@Gox-TsG can induce the enhanced ER stress of cancer cells, which resulted in the higher expression of CRT proteins in ER (Figure 4G,H).

To test the exposure of CRT proteins on the cell membrane, the cells were not permeated after various treatments to preserve the integrity of the cell membrane. Then cells were incubated with anti-CRT-Alex 647, cell membrane tracker, and Hoechst 33 342 in proper order. As shown in Figure 4I,J, the cells treated with PBS and Td@TsG did not expose CRT on the cell membrane, indicating that no ICD of cancer cells was induced. After treated with Td@Gox, the CRT (red) and the cell membrane (green) were co-located together, indicating that the CRT exposed obviously on the cell membrane, which suggested that the ICD of cells was induced. Moreover, the cells have higher CRT exposure on the cell membrane after treated with Td@Gox-TsG, which indicates that the more intense ICD was induced by Td@Gox-TsG. Above experimental results indicated that more intense ER stress resulted in more enhanced ICD of cancer cells by Td@Gox-TsG.

2.7. Visualization of High Mobility Group Box 1 (HMGB1)

HMGB1 is a highly conserved nucleoprotein widely distributed in mammalian cells, which is also the biomarker of ICD.[18] HMGB1-positive nuclear staining showed that HMGB1 mainly distributed in the nucleus when cells were not stimulated (**Figure 5**). When received stimulant (Td@Gox), cells released HMGB1 from the nucleus to the extracellular as a damage-associated molecular pattern, so the fluorescence signal of HMGB1 in nucleus decreased distinctly (Figure 5). As expected, less HMGB1 in the Td@Gox-TsG group was left behind in nucleus, which demonstrated that the cells received more severe stimulant and suffered from more enhanced ICD (Figure 5). The results indicated that our ER-targeted Td@Gox-TsG gave rise to more pronounced irritation and higher ICD-induction efficacy of cells.

2.8. Tumor Targeting In Vivo

To target the tumor and reduce the damage to normal tissues, Td@Gox-TsG was camouflaged by homologous cancer membrane to obtain the "smart bullet" Td@Gox-TsG@C.[19] And the Td@Gox-TsG was modified with a near infrared fluorescent dye (IR 808) to monitor the distribution of our materials. After treated with Td@Gox-TsG or Td@Gox-TsG@C, the mice were measured by an in vivo imaging system at different periods. **Figure 6** showed that the fluorescence signals first increased and then decreased over time, with the maximum fluorescence intensity at 12 h. And the fluorescence intensities of mice treated with Td@Gox-TsG@C were much higher than that with Td@Gox-TsG (Figure 6B,D). The above results demonstrated that our "smart bullet" possessed better targeting ability for tumor tissues.

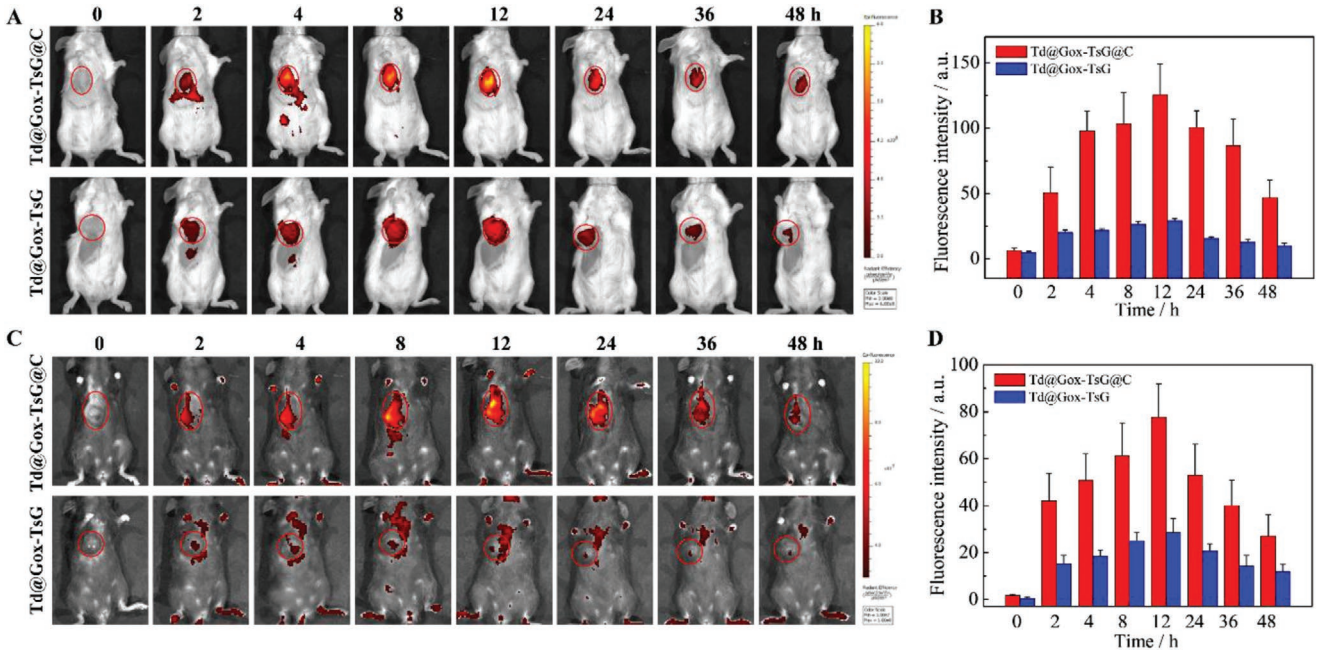

Figure 6. Tumor targeting in vivo. A) Balb/C mice were treated with Td@Gox-TsG or Td@Gox-TsG@C by intravenous injection and measured at different times; B) The corresponding quantifications of fluorescence intensity of tumors ($n = 3$); C) C57 mice were treated with Td@Gox-TsG or Td@Gox-TsG@C (BF cells) by intravenous injection and measured at different times; D) The corresponding quantifications of fluorescence intensity of tumors ($n = 3$).

2.9. Verification of ER Stress and ICD In Vivo

To verify the ER stress and ICD in vivo, the GRP78 and CRT protein of tumors were studied after different treatments. The RT-PCR and western blotting data showed that high GRP78 and CRT protein expressed in the tumors of mice treated with Td@Gox@C, which indicated the induced ER stress and ICD in vivo. And the tumors treated with Td@Gox-TsG@C expressed higher level of GRP78 and CRT than that with Td@Gox@C, which indicated that ER stresses and ICD were more intense by directly stimulating the ER in vivo (Figure S7, Supporting Information). To further verify the induced ICD by Td@Gox-TsG@C in vivo, the immunohistochemistry (IHC) staining analysis for CRT and HMGB1 of tumor tissues of mice after treated with 1) PBS, 2) Td@TsG@C, 3) Td@Gox@C, 4) Td@Gox-TsG@C were studied. As shown in Figure S8A,B, Supporting Information, the more abundant expression of HMGB1 and CRT in the mice treated with Td@Gox@C compared to that with PBS demonstrated that the Td@Gox@C can induce the ICD in vivo. Moreover, the levels of HMGB1 and CRT in mice treated with Td@Gox-TsG@C were higher than that with Td@Gox@C, which indicated that Td@Gox-TsG@C can induce the enhanced ICD in vivo. Since HMGB1 migrates from the nucleus during ER stress, we further measured the level of HMGB1 in serum of mice by enzyme linked immunosorbent assay (ELISA) (Figure S8C,D, Supporting Information). Data showed that the HMGB1 in serum after treated with PBS and Td@TsG@C was in equal level, indicating that no ER stress and ICD occurred. After treated with Td@Gox@C, the HMGB1 in serum evidently increased, which revealed that ER stress and ICD were induced. Significantly, the HMGB1 in serum increased more as treated with Td@Gox-TsG@C than Td@Gox@C, showing that the Td@Gox-TsG@C can induce more intense ER stress and ICD in vivo.

2.10. Dendritic Cell Maturation and Antigen Presentation

Dendritic cells (DCs) are the paramount antigen presenting cells (APCs) to activate T cells, which play the pivotal parts to initiate, regulate, and maintain the immune response.[20] Therefore, the ICD-induced dendritic cell maturation was investigated. Balb/C or C57 mice were provided pretreatment with 1) PBS, 2) Td@TsG@C, 3) Td@Gox@C, 4) Td@Gox-TsG@C, respectively. Then the single cells harvested from lymph nodes were analyzed by flow cytometry assays. **Figure 7**B–E showed that low proportion of mature dendritic cells (CD11+CD80+ and CD11+CD86+ cells) were induced by PBS or Td@TsG@C, indicating their weak immunogenicity. Td@Gox@C gave rise to the moderate mature dendritic cells, while Td@Gox-TsG@C induced remarkable promoted mature dendritic cells. The results indicated that the stimulation in ER was more critical than that in cytoplasm to trigger the immune response.

The antigen presentation in APC has been studied further. The obtained DCs were co-cultured with 1) PBS, 2) Td@TsG@C, 3) Td@Gox@C, 4) Td@Gox-TsG@C-treated BF-OVA cells and studied by flow cytometry. As shown in Figure S9, Supporting Information, the significantly higher SIINFEKL-H_2kb complex on the surfaces of DCs in the group 4 that treated with Td@Gox-TsG@C exhibited the more effective presentation of the ovalbumin (OVA) peptide onto MHC I than other groups. The results confirmed that the ICD induced by Td@Gox-TsG@C can enhance the antigen presentation in APCs.

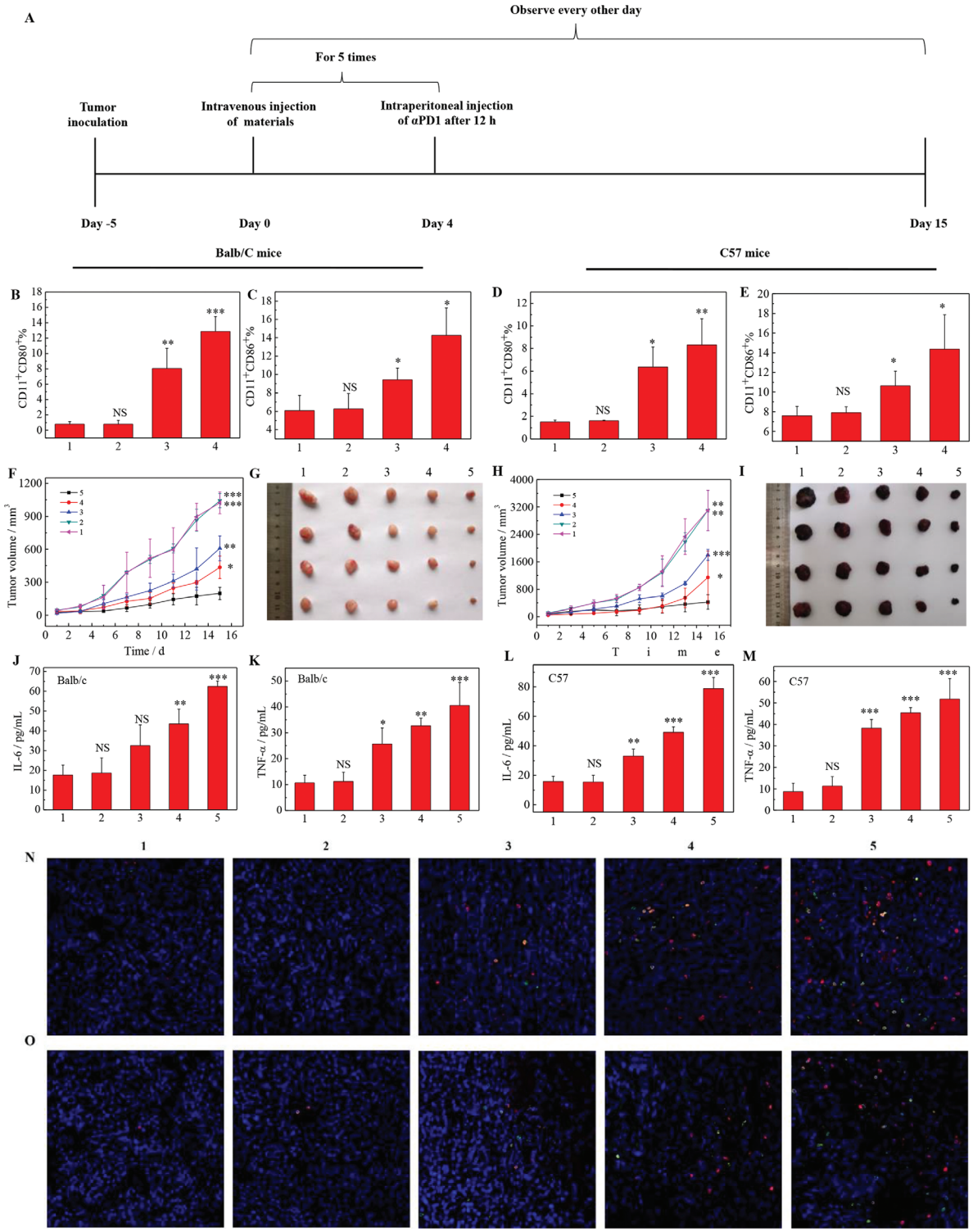

Figure 7. Therapeutic effects in vivo. A) Schematic illustration of the in vivo therapeutic process. Flow cytometric examination of the resultant dendritic cells maturation after different treatments: 1) PBS, 2) Td@TsG@C, 3) Td@Gox@C, 4) Td@Gox-TsG@C: B) CD11+CD80+ cells and C) CD11+CD86+ cells from lymph nodes of Balb/C mice; D) CD11+CD80+ cells and E) CD11+CD86+ cells from lymph nodes of C57 mice. F) The changes of tumor growths and G) pictures of tumors after treatments of Balb/C mice: 1) PBS, 2) Td@TsG@C, 3) Td@Gox@C, 4) Td@Gox-TsG@C, 5) Td@Gox-TsG@C+αPD1; H) The changes of tumor growths and I) pictures of tumors after treatments of C57 mice. J,L) IL-6 and K,M) TNF-α in serum after different treatments (Balb/C and C57 mice, respectively). Immunofluorescence staining images of tumor tissues of N) Balb/C mice and O) C57 mice after treatments: CD3+ (red); CD8+ (green); nucleus (blue). All values in the present study are expressed as means ± SD ($n = 6$). The significance between two groups was analyzed by a two-tailed Student *t*-test (***$p < 0.001$, **$p < 0.01$, *$p < 0.05$, $^{NS}p > 0.05$).

2.11. Therapeutic Effects In Vivo

With superior targeting capability and immunofunction, the antitumor performance of our nanoregulator was evaluated on 4T1 tumor-bearing Balb/C mice and BF tumor-bearing C57 mice. The mice were randomly assigned into five groups respectively and intravenously administrated with: 1) PBS, 2) Td@TsG@C, 3) Td@Gox@C, 4) Td@Gox-TsG@C, 5) Td@Gox-TsG@C+αPD1 (α-PD-1 (αPD1) was intraperitoneally injected 12 h later) for five times totally. The corresponding schematic illustration of therapeutic process in vivo was shown in Figure 7A. As shown in Figure 7F–I, Td@Gox-TsG@C group exhibited greater tumor-inhibiting effect than the Td@Gox@C group, which was due to the enhanced ICD induced by intense ER stress. Although Td@Gox-TsG@C group showed a significant tumor suppression effect in the early stage, tumors tends to grow rapidly in the later period. It was likely owing to the tumor immune escape through the immune checkpoints, which eventually lead to nondurable immune response. Anti-PD1 (α-PD-1 or αPD1), one of the most promising immune checkpoint inhibitors in clinic, can suppress PD-1/PD-L1 axis effectively to prevent the tumor immune escape. More significantly, the enhanced ICD by the nanoregulator would change the immune microenvironment, which makes the tumor more susceptible to the treatment with immune checkpoint inhibitor. Therefore, the immune checkpoint inhibitor (α-PD-1) was applied in this work to assist the nanoregulator for durable and effective immunotherapy. With the synergistic action of α-PD-1, Td@Gox-TsG@C+αPD1 group showed an expectedly enhanced anti-tumor activity during the whole treatment process compared to Td@Gox-TsG@C alone (Figure 7F–I). The corresponding images of mice before and after different treatments (Figure S10, Supporting Information) and tumor weights of the mice after different treatments also indicated the good therapeutic effect (Figure S11, Supporting Information).

As Td@Gox-TsG@C combined with α-PD-1 caused effective suppression of both 4T1 and BF tumors, which we hypothesized was on account of activated immune response, the antitumor immunity was further investigated. Cytokines secretion is one of the most representative symbols during immune responses.[21] The tumor necrosis factor-α (TNF-α) and interleukin-6 (IL-6) in serum were harvested and measured by enzyme-linked immunosorbent assay (ELISA). Although cytokines secretion induced by Td@Gox@C increased evidently, their secretions caused by Td@Gox-TsG@C were much higher, indicating the benefit of our nanoregulator for provoking the immune response (Figure 7J–M). Remarkably, combined with α-PD-1, the level of cytokines increased to the highest among all groups, which demonstrated the strongest immune response. CD3+ and CD8+ T cells in tumors are another representative markers for proofing immune response. Tumors of mice were gained and studied by immunofluorescence staining. Figure 7 N and O showed that Td@Gox-TsG@C+αPD1 groups exhibited the most CD3+ and CD8+ T cells in tumor slides, which indicated the most significant immune response in accordance with the ELISA results.

In view that overmuch cytokines take a risk to damage the normal organs, the safety of Td@Gox-TsG@C were further evaluated in vivo. Figure S12, Supporting Information, showed that all treatments exhibited negligible influence on body weights, which indicated no systemic toxicity of our materials. Serum biochemistry assay of (ALT, AST, BUN, and CR) and haematoxylin and eosin (H&E) staining of major organs (heart, liver, spleen, lung, and kidney) also showed that the vital organs of mice did not exhibit the abnormal after treatments (Figures S13–S15, Supporting Information), indicating the low side effects of our nanoregulator. The above results indicated that such increased cytokines were tolerable during immunotherapy.

3. Conclusion

In summary, we have presented a functionalized nanoregulator based on DNA tetrahedron that specifically induces ER stress for upregulating immunogens and enhancing immunotherapy. This structurally well-defined nanoregulator possesses several outstanding merits. First, "smart bullets" camouflaged by cancer cell membranes can accurately target to homologous tumors. Second, the small-sized DNA nanocarrier is suitable for accumulation in organelle in the assistance of targeted groups. Finally, both glucose depletion and ROS increase induced by Gox in ER can directly cause intense ER stress. Compared with previously reported strategies, the high efficiency of the current approach benefits from the fact that the chemical reaction takes place inside the ER of cancer cells to trigger ER stress. In vivo experiments showed that the effect of immunotherapy was greatly improved after treated with our ER-targeted nanoregulator and checkpoint blockade inhibitor in breast cancer and melanoma models. We hope that this strategy can open new avenues for enhancing tumor immunotherapy by regulating the behavior of cancer cells.

4. Experimental Section

Synthesis of Endoplasmic Reticulum Targets Group (TsG): The compound tosylglycine (TsG) with methyl sulfonamide group and carboxy group was synthesized (named as TsG). In detail, glycine (0.75 g, 10 mmol) was dissolved in a solution of Na_2CO_3 (1.27 g, 12 mmol) in water (15 mL). The mixture was stirred for 5 min and cooled to −5 °C, and then TsCl (2.28 g, 12 mmol) was added for four times in 2 h. The solution was warmed to surrounding temperature and stirred intensely for another 3 h. When completed (determined by TLC, MeOH/DCM, 1:10), the mixture was acidified using 20% HCl to pH 2.0. The turbid liquid was filtered and the crystals were washed by cooled water to obtain the final product. Yield 2.15 g, 94%. ^{1}H NMR (400 MHz, DMSO-d6) δ 7.97–7.93 (t, J = 8 Hz, 1H), 7.69–7.67 (d, J = 8 Hz, 2H), 7.38–7.36 (d, J = 8 Hz, 2H), 3.56–3.55 (d, J = 8 Hz, 2H), 2.38 (s, 3H); ^{13}C NMR (400 MHz, DMSO-d6) δ 170.68, 143.06, 138.27, 129.96, 126.99, 44.23, 21.42. HRMS (ESI) m/z calculated for $C_9H_{10}NO_4S^-$ [(M–H) $^-$]: 228.0336, found: 228.0214.

Synthesis of the DNA Tetrahedron with Amino Groups (Td): Amino group (NH_2)-modified oligonucleotides S1, S2, S3, and S4 were equimolar (2.5 μM) mixed in a TM buffer (20 mM Tris, 50 mM Mg^{2+}, pH 8.0). The mixed solution was incubated at 95 °C for 5 min and then cooled to 4 °C rapidly to form DNA tetrahedron (Td). The Td was stored at 4 °C for further use. Oligonucleotide sequences are shown in Table S1, Supporting Information. The Td modified with fluorescent dye (FAM) was prepared with S1-FAM, S2, S3, and S4 by the same method, which was named as Td-FAM.

Synthesis of the Functional Materials that Induce Endoplasmic Reticulum Stress (Td@Gox-TsG@C): TsG was dissolved in DMSO and then added into 2.4 mL PBS buffer slowly. EDC and NHS were mixed with the above solution to activate the carboxyl groups of TsG (molar ratio, TsG:EDC:NHS = 1:1:1). After 30 min, Gox was added into the solution with stirring at 4 °C overnight. The reaction mixture was centrifugated by ultrafiltration centrifuge tube and washed with PBS buffer to remove the redundant TsG. The obtained substance was named as Gox-TsG.

Next, Gox-TsG was mixed with EDC and NHS to activate the carboxyl groups of Gox. After 30 min, the Td was added into the mixture with stirring at 4 °C overnight. The reaction mixture was centrifugated by ultrafiltration centrifuge tube and washed with PBS buffer to obtain Td@Gox-TsG. The materials without Gox (Td-TsG) or without TsG (Td-Gox) were also prepared to serve as the control.

Then the Td@Gox-TsG was coated with the membrane of cancer cells to achieve Td@Gox-TsG@C. Cancer cells were digested with trypsin and collected by centrifugation (1000 rpm, 3 min). After washed twice with Tris-HCl buffer (pH 7.4), cancer cells were resuspended in Tris-HCl buffer with protease inhibitor (1%) and disrupted with the homogenizer in ice-water bath. The membrane fragments were obtained by differential centrifugation. Membrane fragments were then mixed with Td@Gox-TsG at 4 °C and stirred for 24 h. After centrifugation by ultrafiltration centrifuge tube, the Td@Gox-TsG@C was separated and redispersed in PBS. The Td@TsG or Td@Gox were coated with cancer cell membrane with the same method.

Verification of Membrane Coating by Western Blotting: Cancer cell membrane protein was characterized by the sodium dodecyl sulfate polyacrylamide gel electrophoresis (SDS-PAGE) method. To obtain the protein sample, T-1: 4T1 cells; T-2: cell membrane extracted from 4T1 cells; T-3: Td@Gox-TsG@C (4T1 cell membrane); B-1: BF cells; B-2: cell membrane extracted from BF cells; B-3: Td@Gox-TsG@C (BF cell membrane) were lysed with RIPA lysis buffer. The concentration of protein was quantified using BCA protein assay kit. SDA-PAGE protein loading buffer was added to the protein samples and the mixture was heated with boiling water for 10 min in order to make the protein fully denatured. Subsequently, samples with equal protein amount were added into the wells with 10% SDS-PAGE gel, and SDS-PAGE gel electrophoresis was used to separate protein. Afterward, the proteins were transferred to polyvinylidene difluoride (PVDF) membrane. The membranes were blocked with western blocking buffer shaken slowly on a shaker at room temperature for 60 min and incubated with primary antibody at 4 °C. Then horseradish peroxidase-labeled goat anti-rabbit IgG (H + L) was added with incubation for 1 h. The signals of protein were checked by chemiluminescence enhancement method. The ChemiDoc XRS gel imaging system (bio-rad, Hercules, CA, USA) was used to record information.

Endoplasmic Reticulum Co-Localization: To study the ability of TsG to target to endoplasmic reticulum, the used DNA tetrahedron was modified with FAM (Td-FAM). The cells (4T1 or BF) were treated with materials without TsG or materials with TsG. After incubated for 4 h, the cells were washed with PBS, and then incubated with a commercial endoplasmic reticulum located dye (ER-Tracker Red) for 15 min. Finally, the cells were washed with PBS and studied by confocal laser scanning microscopy.

Then the endoplasmic reticulum colocalization was verified by flow cytometry. The cells (4T1 or BF) were treated with materials with TsG. for 4 h and then digested with trypsin. After incubated with ER-Tracker Red for 15 min, the cells were centrifugated (1000 rpm, 3 min) and washed with PBS. Then the cells were studied by flow cytometry.

Evaluation of Intracellular Reactive Oxygen Species: 4T1 or BF cells were divided into four groups and treated with: 1, PBS buffer (PBS); 2, Td@TsG; 3, Td@Gox; 4, Td@Gox-TsG, respectively. After 4 h, the cells were incubated with DCFH for 10 min. Then the cells were washed with PBS and studied by confocal laser scanning microscopy.

Evaluation of Calreticulin: The immunofluorescence staining was performed to study the CRT of 4T1 and BF cells with different treatments. Cells were divided into four groups and incubated with: 1, PBS; 2, Td@TsG; 3, Td@Gox; 4, Td@Gox-TsG for 4 h. Then the cells were fixed and permeated before treated with blocking reagent. Cells were stained with anti-CRT-Alex 647 in the dark overnight at 4 °C. After stained with Hoechst 33 342 and treated with anti-fluorescence quenching agent, cells were studied by confocal fluorescence imaging.

CRT was also studied by flow cytometry. 4T1 cells were divided into four groups and incubated with: 1, PBS; 2, Td@TsG; 3, Td@Gox; 4, Td@Gox-TsG for 4 h. Cells were digested with trypsin and collected by centrifugation (1000 rpm, 3 min). Then cells were treated with anti-CRT-Alex 647 for 30 min and studied by flow cytometry after washed with PBS.

Evaluation of High Mobility Group Protein (HMGB1) in Cell Nucleus: The immunofluorescence staining was performed to study the high mobility group protein (HMGB1) of 4T1 and BF cells with different treatments. Cells were divided into four groups and incubated with: 1, PBS; 2, Td@TsG; 3, Td@Gox; 4, Td@Gox-TsG for 4 h. Then the cells were washed with PBS and cultured with fresh 1640 medium for another 12 h. Cells were fixed and permeated before treated with blocking reagent. Then cells were stained with primary antibodies (anti-HMGB1) overnight at 4 °C. After washed with PBS, cells were stained with the second antibody (with DyLight 550) for 1 h in the dark and then incubated with Hoechst 33 342. After washed and treated with anti-fluorescence quenching agent, cells were studied by confocal fluorescence imaging.

Evaluation of Glucose-Regulated Protein 78 (GRP78): 4T1 or BF cells were divided into four groups and incubated with: 1, PBS; 2, Td@TsG; 3, Td@Gox; 4, Td@Gox-TsG for 4 h. Then the cells were washed, fixed, and permeated before treated with blocking reagent. Then cells were stained with primary antibodies (anti-GRP78) overnight at 4 °C. After washed with PBS, cells were stained with the second antibody (with DyLight 550) for 1 h in the dark and then incubated with Hoechst 33 342. After washed and treated with anti-fluorescence quenching agent, cells were studied by confocal fluorescence imaging.

Tumor Targeting In Vivo Assay: To study the tumor target ability to the tumor, the Td@Gox-TsG were modified with a near infrared fluorescent dye (IR 808). Female Balb/C mice with 4T1 tumor were divided into two groups and injected intravenously with Td@Gox-TsG or Td@Gox-TsG@C (4T1 cell membrane), respectively. The mice were measured by an in vivo imaging system (IVIS) at different times. Female C57 mice with BF tumor were also studied by intravenous injection with Td@Gox-TsG or Td@Gox-TsG@C (BF cell membrane), the same as above.

Dendritic Cell Maturation and Antigen Presentation: To analyze the maturation of dendritic cells, female Balb/C mice with 4T1 tumors were divided into four groups and injected intravenously with 1, PBS; 2, Td@TsG@C; 3, Td@Gox@C; 4, Td@Gox-TsG@C. Mice were sacrificed and the lymph nodes were harvested to obtain the single cell. In brief, the lymph nodes were decomposed into smaller chunks and placed into a glass homogenizer containing PBS buffer (pH 7.4) with 2% heat-inactivated FBS. Next, a single cell suspension was obtained by gentle pressure with the homogenizer without adding digestive enzyme. Then, red blood cells (RBCs) in the single cell suspension were removed with RBC lysis buffer. Finally, the obtained single cells were stained with fluorescence-labeled antibodies: anti-CD11-FITC and anti-CD80-PE; anti-CD11-FITC and anti-CD86-APC antibodies according to the manufacturer's protocols. All the antibodies in the experiments were used following the protocols recommended by the manufacturer. The cells were studied by flow cytometry. The activation of dendritic cells of female C57 mice with BF tumors were also studied by the same method.

The antigen presentation in APC has been studied further. DCs, the most powerful APC, were obtained from the bone marrow of C57 mice and cultured with 50 ng mL^{-1} GM-CSF and 50 ng mL^{-1} IL-4.[22] The obtained DCs were cocultured with 1) PBS, 2) Td@TsG@C, 3) Td@Gox@C, 4) Td@Gox-TsG@C-treated BF-OVA cells. After 24 h, the cells were washed and stained with anti-CD11-FITC and anti-SIINFEKL/H-2Kb (25-D1.16)-PE-Cyanine7 and then studied by flow cytometry.

Tumor Therapy Experiment: For the xenografts established from cultured cells, 4T1 cells (or BF cells) were suspended and harvested after trypsinization, and approximately 5×10^5 4T1 cells in 50 µL of serum-free RPMI 1640 medium were subcutaneously injected into the right flank of the Balb/C mice (or BF mice). The tumor volume (V) was determined by measuring the length (L) and width (W) and was calculated as $L \times W^2/2$.

To study the antitumor efficacy, mice with tumors were randomly divided into five groups ($n = 6$) and subjected to different treatments: 1, PBS; 2, Td@TsG@C; 3, Td@Gox@C; 4, Td@Gox-TsG@C; 5, intravenously injected with Td@Gox-TsG@C and then intraperitoneally injected with a-PD-1 (200 μg each time) 12 h later (Td@Gox-TsG@C+aPD1). The intravenously injected dose was 10 mg kg^{-1} (according to the amount of Gox) each time for five times in total. The tumor volumes and body weights of the mice were measured every other day for 14 days. Blood biochemical test (ALT, AST, BUN, CR) and H&E staining of the five major organs (heart, liver, spleen, lung, and kidney) were carried out at 12 h post-treatment to prove that the body's immune response resulted in minimal side effects to major organs. The tumors of mice were harvested to evaluate the infiltrated CD8+ T cells by immunofluorescence analysis.

ELISA Analysis: Serum cytokine levels were determined by enzyme-linked immunosorbent assays (ELISAs) using antibody pairs specific to these cytokines, following protocols recommended by the manufacturer. Mice with tumors were divided into six groups ($n = 6$) and subjected to different treatments: 1, PBS; 2, Td@TsG@C; 3, Td@Gox@C; 4, Td@Gox-TsG@C; 5, Td@Gox-TsG@C+aPD1. After 12 h, the mice were sacrificed to harvest serum. Serum levels of IL-6 and TNF-α were determined with the Mouse IL-6 ELISA Kit and TNF-α Mini ELISA Kit, respectively.

Statistical Analysis: All values in the present study were expressed as means ± SD. The significance between two groups was analyzed by a two-tailed Student *t*-test. *p*-value of less than 0.05 was considered significant (***$p < 0.001$, **$p < 0.01$, *$p < 0.05$).

Supporting Information

Supporting Information is available from the Wiley Online Library or from the author.

Acknowledgements

This work was supported by Key Research and Development Program of Shandong Province (2018YFJH0502), National Natural Science Foundation of China (91753111, 21927881, 21874086, and 21775094), National Key R&D Program of China (2019YFA0210100), and Youth Innovation Science and Technology Program of Higher Education Institution of Shandong Province (2019KJC022). Animal experiments were reviewed and approved by the Ethics Committee of Shandong Normal University, Jinan, P. R. China (approval number AEECSDNU 2019030). All the animal experiments complied with relevant guidelines of the Chinese government and regulations for the care and use of experimental animals.

Conflict of Interest

The authors declare no conflict of interest.

Author Contributions

The manuscript was written through contributions of all authors. All authors have given approval to the final version of the manuscript.

Keywords

calreticulin proteins, DNA tetrahedron, endoplasmic reticulum stress, immunotherapies, nanoregulators

Received: January 19, 2020
Revised: August 24, 2020
Published online:

[1] a) A. Ribas, J. D. Wolchok, *Science* **2018**, *359*, 1350; b) N. Nagarsheth, M. S. Wicha, W. Zou, *Nat. Rev. Immunol.* **2017**, *17*, 559; c) P. Gotwals, S. Cameron, D. Cipolletta, V. Cremasco, A. Crystal, B. Hewes, B. Mueller, S. Quaratino, C. Sabatos-Peyton, L. Petruzzelli, J. A. Engelman, G. l. Dranoff, *Nat. Rev. Cancer* **2017**, *17*, 286; d) B. Routy, E. L. Chatelier, L. Derosa, C. P. M. Duong, M. T. Alou, R. Daillère, A. Fluckiger, M. Messaoudene, C. Rauber, M. P. Roberti, M. Fidelle, C. Flament, V. Poirier-Colame, P. Opolon, C. Klein, K. Iribarren, L. Mondragón, N. Jacquelot, B. Qu, G. Ferrere, C. Clémenson, L. Mezquita, J. R. Masip, C. Naltet, S. Brosseau, C. Kaderbhai, C. Richard, H. Rizvi, F. Levenez, N. Galleron, et al., *Science* **2018**, *359*, 91; e) C. H. June, R. S. O'Connor, O. U. Kawalekar, S. Ghassemi, M. C. Milone, *Science* **2018**, *359*, 1361; f) K. M. Mahoney, P. D. Rennert, G. J. Freeman, *Nat. Rev. Drug Discov.* **2015**, *14*, 561.

[2] a) M. M. Gubin, R. D. Schreiber, *Science* **2015**, *350*, 158; b) B. A. Johnson, M. Yarchoan, V. Lee, D. A. Laheru, E. M. Jaffee, *Clin. Cancer Res.* **2017**, *23*, 1656; c) B. Feng, F. Zhou, B. Hou, D. Wang, T. Wang, Y. Fu, Y. Ma, H. Yu, Y. Li, *Adv. Mater.* **2018**, *30*, 1803001.

[3] a) Q. V. Le, J. Suh, J. J. Choi, G. T. Park, J. W. Lee, G. Shim, Y. K. Oh, *ACS Nano* **2019**, *13*, 7442; b) S. K. Horrevorts, J. J. Garcia-Vallejo, S. J. van Vliet, A. A. van de Loosdrecht, Y. van Kooyk, T. D. de Gruijl, *Immunotherapy* **2016**, *8*, 5; c) H. Di-Hwei, P. Pedro, V. Gilbert, R. Alberto, M. D. Anita, A. Eric, Z. Laurence, L. P. Jean-Bernard, *J. Immunother.* **2003**, *26*, 440; d) J. Saenz-Badillos, S. P. Amin, R. D. Granstein, *Exp. Dermatol.* **2001**, *10*, 143; e) M. Vergati, C. Intrivici, N. Y. Huen, J. Schlom, K. Y. Tsang, *BioMed Res. Int.* **2010**, *2010*, 596432.

[4] a) G. Kroemer, L. Galluzzi, O. Kepp, L. Zitvogel, *Annu. Rev. Immunol.* **2013**, *31*, 51; b) D. V. Krysko, A. D. Garg, A. Kaczmarek, O. Krysko, P. Agostinis, P. Vandenabeele, *Nat. Rev. Cancer* **2012**, *12*, 860; c) L. Galluzzi, A. Buqué, O. Kepp, L. Zitvogel, G. Kroemer, *Nat. Rev. Immunol.* **2017**, *17*, 97; d) L. Bezu, L. C. Gomes-da-Silva, H. Dewitte, K. Breckpot, J. Fucikova, R. Spisek, L. Galluzzi, O. Kepp, G. Kroemer, *Front. Immunol.* **2015**, *6*, 187; e) Y. Yang, J. Tang, P. L. Abbaraju, M. Jambhrunkar, H. Song, M. Zhang, C. Lei, J. Fu, Z. Gu, Y. Liu, C. Yu, *Angew. Chem.* **2018**, *130*, 11938; f) C. He, X. Duan, N. Guo, C. Chan, C. Poon, R. R. Weichselbaum, W. Lin, *Nat. Commun.* **2016**, *7*, 12499; g) M. Obeid, A. Tesniere, F. Ghiringhelli, G. M. Fimia, L. Apetoh, J. L. Perfettini, M. Castedo, G. Mignot, T. Panaretakis, N. Casares, D. Métivier, N. Larochette, P. v. Endert, F. Ciccosanti, M. Piacentini, L. Zitvogel, G. Kroemer, *Nat. Med.* **2007**, *13*, 54.

[5] G. I. Evan, K. H. Vousden, *Nature* **2001**, *411*, 342.

[6] a) L. Galluzzi, A. Buqué, O. Kepp, L. Zitvogel, G. Kroemer, *Nat. Rev. Immunol.* **2017**, *17*, 97; b) G. Kroemer, L. Galluzzi, O. Kepp, L. Zitvogel, *Annu. Rev. Immunol.* **2013**, *31*, 51.

[7] a) T. Panaretakis, O. Kepp, U. Brockmeier, A. Tesniere, A. Bjorklund, D. C. Chapman, M. Durchschlag, N. Joza, G. Pierron, P. v. Endert, J. Yuan, L. Zitvogel, F. Madeo, D. B. Williams, G. Kroemer, *EMBO J.* **2009**, *28*, 578; b) A. D. Garg, D. V. Krysko, T. Verfaillie, A. Kaczmarek, G. B. Ferreira, T. Marysael, N. Rubio, M. Firczuk, C. Mathieu, A. J. M. Roebroek, W. Annaert, J. Golab, P. d. Witte, P. Vandenabeele, P. Agostinis, *EMBO J.* **2012**, *31*, 1062.

[8] C. Chen, X. Ni, S. Jia, Y. Liang, X. Wu, D. Kong, D. Ding, *Adv. Mater.* **2019**, *31*, 1904914.

[9] a) C. Guo, R. Ma, X. Liu, Y. Xia, P. Niu, J. Ma, X. Zhou, Y. Li, Z. Sun, *Chemosphere* **2018**, *210*, 183; b) C. Xu, B. Bailly-Maitre, J. C. Reed, *J. Clin. Invest.* **2005**, *115*, 2656; c) I. Tabas, D. Ron, *Nat. Cell Biol.* **2011**, *13*, 184; d) I. Kim, W. Xu, J. C. Reed, *Nat. Rev. Drug Discov.* **2008**, *7*, 1013.

[10] a) R. Wilson, A. P. F. Turner, *Biosens. Bioelectron.* **1992**, *7*, 165; b) S. B. Bankar, M. V. Bule, R. S. Singhal, L. Ananthanarayan, *Biotechnol. Adv.* **2009**, *27*, 489.

[11] a) Y. Li, N. Li, W. Pan, Z. Yu, L. Yang, B. Tang, *ACS Appl. Mater. Interfaces* **2017**, *9*, 2123; b) N. Li, Z. Yu, W. Pan, Y. Han, T. Zhang, B. Tang, *Adv. Funct. Mater.* **2013**, *23*, 2255.
[12] a) T. Wu, J. Liu, M. Liu, S. Liu, S. Zhao, R. Tian, D. Wei, Y. Liu, Y. Zhao, H. Xiao, B. Ding, *Angew. Chem., Int. Ed.* **2019**, *58*, 14224; b) J. Zhang, Y. Guo, F. Ding, G. Pan, X. Zhu, C. Zhang, *Angew. Chem.* **2019**, *131*, 13932.
[13] a) J. T. Hou, H. S. Kim, C. Duan, M. S. Ji, S. Wang, L. Zeng, W. X. Ren, J. S. Kim, *Chem. Commun.* **2019**, *55*, 2533; b) H. Xiao, C. Wu, P. Li, W. Gao, W. Zhang, W. Zhang, L. Tong, B. Tang, *Chem. Sci.* **2017**, *8*, 7025.
[14] N. Li, M. Wang, X. Gao, Z. Yu, W. Pan, H. Wang, B. Tang, *Anal. Chem.* **2017**, *89*, 6670.
[15] L. H. Fu, C. Qi, J. Lin, P. Huang, *Chem. Soc. Rev.* **2018**, *47*, 6454.
[16] K. Xu, M. Qiang, W. Gao, R. Su, N. Li, Y. Gao, Y. Xie, F. Kong, B. Tang, *Chem. Sci.* **2013**, *4*, 1079.
[17] a) Y. L. Tsai, D. P. Ha, H. Zhao, A. J. Carlos, S. Wei, T. K. Pun, K. Wu, E. Zandi, K. Kelly, A. S. Lee, *Proc. Natl. Acad. Sci. U. S. A.* **2018**, *115*, E4245; b) M. Prasad, K. J. Pawlak, W. E. Burak, E. E. Perry, B. Marshall, R. M. Whittal, H. S. Bose, *Sci. Adv.* **2017**, *3*, e1602038.
[18] H. Yang, H. Wang, S. S. Chavan, U. Andersson, *Mol. Med.* **2015**, *21*, S6.
[19] a) Z. Yu, P. Zhou, W. Pan, N. Li, B. Tang, *Nat. Commun.* **2018**, *9*, 5044; b) H. Sun, J. Su, Q. Meng, Q. Yin, L. Chen, W. Gu, P. Zhang, Z. Zhang, H. Yu, S. Wang, Y. Li, *Adv. Mater.* **2016**, *28*, 9581.
[20] A. V. Kroll, R. H. Fang, Y. Jiang, J. Zhou, X. Wei, C. L. Yu, J. Gao, B. T. Luk, D. Dehaini, W. Gao, L. Zhang, *Adv. Mater.* **2017**, *29*, 1703969.
[21] J. J. O'Shea, A. Ma, P. Lipsky, *Nat. Rev. Immunol.* **2002**, *2*, 37.
[22] a) D. Sichien, B. N. Lambrecht, M. Guilliams, C. L. Scott, *Mucosal Immunol.* **2017**, *10*, 831; b) M. B. Lutz, N. Kukutsch, A. L. J. Ogilvie, S. Rößner, F. Koch, N. Romani, G. Schuler, *J. Immunol. Methods* **1999**, *223*, 77.